



A new method for inverse electromagnetic casting problems based on the topological derivative

Alfredo Canelas, Novotny Andre Antonio, Jean Rodolphe Roche

► To cite this version:

Alfredo Canelas, Novotny Andre Antonio, Jean Rodolphe Roche. A new method for inverse electromagnetic casting problems based on the topological derivative. *Journal of Computational Physics*, 2011, 230 (9), pp.3570-3588. 10.1016/j.jcp.2011.01.049 . hal-01276442

HAL Id: hal-01276442

<https://hal.science/hal-01276442>

Submitted on 22 Feb 2016

HAL is a multi-disciplinary open access archive for the deposit and dissemination of scientific research documents, whether they are published or not. The documents may come from teaching and research institutions in France or abroad, or from public or private research centers.

L'archive ouverte pluridisciplinaire **HAL**, est destinée au dépôt et à la diffusion de documents scientifiques de niveau recherche, publiés ou non, émanant des établissements d'enseignement et de recherche français ou étrangers, des laboratoires publics ou privés.

A New Method for Inverse Electromagnetic Casting Problems Based on the Topological Derivative

Alfredo Canelas^a, Antonio A. Novotny^b, Jean R. Roche^c

^a*Instituto de Estructuras y Transporte, Facultad de Ingeniería, UDELAR, J. Herrera y Reissig 565, CP 11300, Montevideo, Uruguay*

^b*Laboratório Nacional de Computação Científica LNCC/MCT, Av. Getúlio Vargas 333, 25651-075, Petrópolis - RJ, Brasil*

^c*Institut Elie Cartan de Nancy, Nancy-Université, CNRS, INRIA, B.P. 70239, 54506, Vandoeuvre lès Nancy, France*

Abstract

The inverse electromagnetic casting problem consists in looking for a suitable set of electric wires such that the electromagnetic field induced by an alternating current passing through them, makes a given mass of liquid metal acquire a predefined shape. In this paper we propose a method for the topology design of such inductors. The inverse electromagnetic casting problem is formulated as an optimization problem, and topological derivatives are considered in order to locate new wires in the right position. Several numerical examples are presented showing that the proposed technique is effective to design suitable inductors.

Keywords: Topological asymptotic analysis, topological derivatives, inverse problem, electromagnetic casting

1. Introduction

The industrial technique of electromagnetic casting allows for contactless heating, shaping and controlling of chemical aggressive, hot melts. The main advantage over the conventional crucible shape forming is that the liquid metal does not come into contact with the crucible wall, so there is no

Email addresses: `acanelas@fing.edu.uy` (Alfredo Canelas), `novotny@lncc.br` (Antonio A. Novotny), `roche@iecn.u-nancy.fr` (Jean R. Roche)

danger of contamination. This is very important in the preparation of very pure specimens in metallurgical experiments, as even small traces of impurities, such as carbon and sulphur, can affect the physical properties of the sample. Industrial applications are, for example, electromagnetic shaping of aluminum ingots using soft-contact confinement of the liquid metal, electromagnetic shaping of components of aeronautical engines made of superalloy materials (Ni,Ti, . . .), control of the structure solidification, etc. [1, 2].

The direct problem consists in determining the resulting liquid metal shape for a known external current distribution. In general, the direct problem can be solved either directly studying the equilibrium equation at the interface, or minimizing an appropriate energy functional, the main advantage of this last method being that the resulting shapes are then mechanically stable [3, 4, 5].

The inverse problem consists in determining the exterior field, and therefore the external currents, for which the liquid metal takes on a given desired shape. The model considered here concerns a vertically falling molten metal column shaped by an externally applied magnetic field created by a set of inductors. In this two-dimensional case, the inverse shaping problem consists in finding a distribution of inductors in order that the generated exterior field makes the horizontal cross-section of the molten metal attain a prescribed shape. This is a very important problem that one needs to solve in order to define a process of electromagnetic liquid metal forming.

In a previous work we studied the inverse electromagnetic shaping problem considering the case where the inductors are made of single solid-core wires with a negligible area of the cross-section [6]. Thus, the inductors were represented by points in the horizontal plane. In a second paper we considered the more realistic case where each inductor is a set of bundled insulated strands [7]. In both cases the number of inductors was fixed in advance. In this paper we aim to overcome this constraint, and look for configurations of inductors considering different topologies with the purpose of obtaining better results. In order to manage this new situation we introduce a new formulation for the inverse problem using a shape functional based on the Kohn-Vogelius criterion, see [8, 9? , 10?]. A topology optimization procedure is defined by means of topological derivatives.

The remaining contents of this paper are organized as follows. The next section describes the direct free-surface problem concerning the electromagnetic casting. Section 3 introduces the topological derivative concept. Section 4 introduces the inverse problem in electromagnetic casting, describes

how to formulate this problem as an optimization problem and shows how to compute the topological derivative of the objective functional. The numerical method proposed here to construct the solution using the topological derivative is detailed in Section 5. Some examples are presented in Section 6 to show the efficacy of the proposed approach. Finally, the conclusions of this paper are presented in Section 7.

2. The mathematical model of the electromagnetic shaping problem

The simplified model of the electromagnetic shaping problem studied here concerns the case of a vertical column of liquid metal falling down into an electromagnetic field created by vertical inductors. We assume that the frequency of the imposed current is very high so that the magnetic field does not penetrate into the metal. In other words, we neglect the skin effect. Moreover, we assume that a stationary horizontal section is reached so that the 2-dimensional model is valid. The equilibrium of the system is ensured by the static balance on the surface of the metal between the surface tension and the electromagnetic forces. This problem and other similar ones have been considered by several authors, we refer the reader to the following papers for the physical analysis of the simplifying assumptions of the model: see [11, 12, 13, 3, 14, 15, 4].

We denote by Ω the exterior in the plane of the closed and simply connected domain ω occupied by the cross-section of the metal column. The exterior magnetic field can be found as the solution of the following boundary value problem:

$$\left\{ \begin{array}{ll} \nabla \times \mathbf{B} &= \mu_0 \mathbf{J} & \text{in } \Omega, \\ \nabla \cdot \mathbf{B} &= 0 & \text{in } \Omega, \\ \mathbf{B} \cdot \mathbf{n} &= 0 & \text{on } \Gamma, \\ \|\mathbf{B}(x)\| &= O(\|x\|^{-1}) \text{ as } \|x\| \rightarrow \infty & \text{in } \Omega. \end{array} \right. \quad (1)$$

Here the fields $\mathbf{J} = (0, 0, j_0)$ and $\mathbf{B} = (B_1, B_2, 0)$ represent the mean square values of the current density vector and the total magnetic field, respectively. The constant μ_0 is the vacuum permeability, \mathbf{n} the unit normal vector to the boundary Γ of Ω and $\|\cdot\|$ denotes the Euclidean norm. We assume that j_0 has compact support in Ω and satisfies:

$$\int_{\Omega} j_0 \, dx = 0. \quad (2)$$

Besides, the cross-section area of the liquid metal column is known and equal to S_0 :

$$\int_{\omega} dx = S_0. \quad (3)$$

On the other hand, the magnetic field produces a surface pressure that acts on the liquid metal changing its shape until the equilibrium is attained. The equilibrium is characterized by the following equation [15, 16 ? ?]:

$$\frac{1}{2\mu_0} \|\mathbf{B}\|^2 + \sigma \mathcal{C} = p_0 \quad \text{on } \Gamma, \quad (4)$$

where \mathcal{C} is the curvature of Γ seen from the metal, σ is the surface tension of the liquid and the constant p_0 is an unknown of the problem. Physically, p_0 represents the difference between the internal and external pressures.

In the direct problem the electric current density j_0 is given and one needs to find the shape of ω that satisfies (3) and such that the magnetic field \mathbf{B} solution of (1) satisfies also the equilibrium equation (4) for a real constant p_0 .

Conditions (1)-(2), with the function j_0 compactly supported in Ω , imply the existence of the flux function $\varphi : \Omega \rightarrow \mathbb{R}$ such that $\mathbf{B} = (\frac{\partial \varphi}{\partial x_2}, -\frac{\partial \varphi}{\partial x_1}, 0)$, with φ solution of:

$$\begin{cases} -\Delta \varphi = \mu_0 j_0 & \text{in } \Omega, \\ \varphi = 0 & \text{on } \Gamma, \\ \varphi(x) = c + o(1) & \text{as } \|x\| \rightarrow \infty. \end{cases} \quad (5)$$

This equation have a unique solution in the space $W_0^1(\Omega)$ defined as [17]:

$$W_0^1(\Omega) = \{u : \rho u \in L^2(\Omega) \text{ and } \nabla u \in L^2(\Omega)\}, \quad (6)$$

with $\rho(x) = [\sqrt{1 + \|x\|^2} \log(2 + \|x\|^2)]^{-1}$. The constant c of the condition at infinity in (5) is also an unknown, which has a unique solution in \mathbb{R} . Equivalent formulations of the conditions at infinity are $\varphi(x) = O(1)$ and $\varphi(x) = c + O(1/\|x\|)$ [18]. The form used in (5) is the most convenient in the development of numerical methods of solution.

The solution φ of the exterior problem (5) satisfies the following Poincaré type inequality: there exist a constant $C > 0$ such that [17]

$$\|\varphi\|_{W_0^1(\Omega)} \leq C \|\nabla \varphi\|_{L^2(\Omega)} \quad (7)$$

where the norm $\|\cdot\|_{W_0^1(\Omega)}$ comes from the scalar product of the Hilbert space $W_0^1(\Omega)$:

$$(u, v)_{W_0^1(\Omega)} = \int_{\Omega} \nabla u \cdot \nabla v \, dx + \int_{\Omega} \rho^2 u v \, dx \quad (8)$$

The equilibrium equation (4) in terms of the flux becomes:

$$\frac{1}{2\mu_0} \left| \frac{\partial \varphi}{\partial n} \right|^2 + \sigma \mathcal{C} = p_0 \quad \text{on } \Gamma. \quad (9)$$

The direct problem, in terms of the flux, consists in looking for a domain ω such that the solution φ of (5) satisfies (9) for a real constant p_0 .

3. Topological derivative concept

The topological derivative measures the sensitivity of a given shape functional with respect to an infinitesimal singular domain perturbation, such as the insertion of holes, inclusions, source-terms or even cracks. The topological derivative was rigorously introduced by Sokołowski & Żochowski 1999 [19]. Since then, this concept has proved extremely useful in the treatment of a wide range of problems, namely, topology optimization [20, 21, 22, 23, 24, 25], inverse analysis [26, 27, 28, 29, 30] and image processing [31, 32, 33, 34, 35], and has become a subject of intensive research. Concerning the theoretical development of the topological asymptotic analysis, the reader may refer to the papers [36, 37, 38, 39, 40, 41, 42, 43, 44, 45, 46, 47, 48, 49], for instance.

More precisely, let us consider that the domain Ω is subject to a non-smooth perturbation confined in a small ball $B_\varepsilon(\hat{x})$ of radius ε and center $\hat{x} \in \Omega$. Then, we assume that a given shape functional $\psi(\varepsilon)$, associated to the topologically perturbed domain, admits the following topological asymptotic expansion [19]

$$\psi(\varepsilon) = \psi(0) + f(\varepsilon) D_T \psi + o(f(\varepsilon)), \quad (10)$$

where $\psi(0)$ is the shape functional associated to the original (unperturbed) domain and $f(\varepsilon)$ is a positive function such that $f(\varepsilon) \rightarrow 0$, when $\varepsilon \rightarrow 0$. The function $\hat{x} \mapsto D_T \psi(\hat{x})$ is called the topological derivative of ψ at \hat{x} . Therefore, this derivative can be seen as a first order correction of $\psi(0)$ to approximate $\psi(\varepsilon)$. In fact, the topological derivative $D_T \psi$ is a scalar function

defined over the original domain that indicates, at each point, the sensitivity of the shape functional when a singular perturbation of size ε is introduced at that point.

In this paper we propose a new method for inverse electromagnetic casting problem based on the topological asymptotic expansion (10), which is presented in details in the next section.

4. The Inverse Problem

The goal of the inverse problem is to find a distribution of current around the liquid metal column so that it attains a given shape. In addition, the magnetic field has to be created by a simple configuration of inductors. We consider a distribution of the electric current density j_0 of the form:

$$j_0 = I \sum_{p=1}^m \alpha_p \chi_{\Theta_p}, \quad (11)$$

where I is a predefined intensity of current, Θ_p , with $1 \leq p \leq m$, are bounded domains, χ_{Θ_p} are their characteristic functions, and $\alpha_p \pm 1$. Note that the expression (11) assumes that the electric current density is uniform on each region Θ_p . Inductors made of bundled insulated strands allow the use of (11) as a good approximation, see [50] and references therein.

Therefore, we have to determine the position and shape of the domains Θ_p , $1 \leq p \leq m$, of (11), where m is also an unknown, in such a way that the solution \mathbf{B} of (1) satisfies also the equilibrium equation (4). This topic has been already studied and there are a few number of papers about the existence of solutions, see [13, 51]. **Although these above-mentioned references constitute a great insight on the existence issue, we are also interested in obtaining approximate solutions for situations where the existence of solutions is not ensured. There are also two other reasons that lead us to reject the idea of an algorithm for obtaining exact solutions. First, to the author's knowledge, there is not a complete treatise about the characterization of the solution set, and the uniqueness of the solution in terms of j_0 can not be ensured. Second, unlike the direct problem, the inverse problem is inherently ill posed: small variation of the liquid boundary may cause dramatic variations in the applied exterior field [13, 51].**

These reasons motivates us to formulate the inverse problem as an optimization problem, in order to look for a solution minimizing an appropriate

functional. There are, however, some known facts about the exact solutions of the inverse problem that are of main importance in what follows. It has been shown [13] that the magnetic field \mathbf{B} is the unique analytic extension of the field $\mathbf{B} \cdot \boldsymbol{\tau}$ defined on the boundary Γ of the liquid metal ($\boldsymbol{\tau}$ being the unit tangent vector to Γ). In [13], the authors proved that a solution of (1) and (4) for \mathbf{B} exists only if Γ is an analytic curve, and the function $\mathbf{B} \cdot \boldsymbol{\tau}$ is analytic. Furthermore, from (4) it is possible to show the following:

$$\mathbf{B} \cdot \boldsymbol{\tau} = \varkappa \sqrt{2\mu_0(p_0 - \sigma\mathcal{C})} \quad \text{with} \quad \varkappa = \pm 1. \quad (12)$$

The constant p_0 must satisfy $p_0 \geq \max_{\Gamma} \sigma\mathcal{C}$. If $p_0 > \max_{\Gamma} \sigma\mathcal{C}$ then \varkappa should be constant on Γ . That situation is not possible if (2) is satisfied, see [13]. Hence we have the important result:

$$p_0 = \max_{\Gamma} \sigma\mathcal{C}. \quad (13)$$

Another restriction is imposed on Γ since \varkappa may change the sign at points where $\mathbf{B} \cdot \boldsymbol{\tau} = 0$ (i.e. where \mathcal{C} attains its global maximum), depending on the multiplicity order of these zero points: if the multiplicity order of a zero point is even, \varkappa remains constant. On the other hand, if the multiplicity order of a zero point is odd, \varkappa changes the sign. Hence, by the periodicity of \varkappa , the number of zero points of odd order must be even. For example, any curve which has the curvature attaining its maximum value at an odd number of points (at which $\mathbf{B} \cdot \boldsymbol{\tau}$ has non-degenerate zeros), is in fact impossible to form.

Therefore, calling $\bar{p} = \sqrt{2\mu_0(p_0 - \sigma\mathcal{C})}$, with p_0 known and given by (13), the equilibrium constraint in terms of the flux function reads

$$\frac{\partial \varphi}{\partial n} = \varkappa \bar{p} \quad \text{on } \Gamma, \quad (14)$$

where $\varkappa = \pm 1$, with the sign changes located at points where the curvature of Γ is a global maximum. Of course we have two possible ways to define \varkappa , however, both lead to the same solution j_0 but with the opposite sign.

4.1. Problem Formulation

The previous considerations allow us to formulate the inverse problem as follows: determine the electric current density j_0 and the real constant c in

such a way that the system

$$\begin{cases} -\Delta\varphi = \mu_0 j_0 & \text{in } \Omega, \\ \varphi = 0 & \text{on } \Gamma, \\ \frac{\partial\varphi}{\partial n} = \varkappa \bar{p} & \text{on } \Gamma, \\ \varphi(x) = c + o(1) & \text{as } \|x\| \rightarrow \infty. \end{cases} \quad (15)$$

has a solution $\varphi \in W_0^1(\Omega)$. Let us introduce a shape functional based on the Kohn-Vogelius criterion, namely

$$\psi(0) = J(\phi) = \frac{1}{2} \|\phi\|_{L^2(\Gamma)}^2 = \frac{1}{2} \int_{\Gamma} |\phi|^2 ds, \quad (16)$$

where the auxiliary function ϕ depends implicitly on j_0 and c by solving the following boundary-value problem

$$\begin{cases} -\Delta\phi = \mu_0 j_0 & \text{in } \Omega, \\ \frac{\partial\phi}{\partial n} = \varkappa \bar{p} & \text{on } \Gamma, \\ \phi(x) = c + o(1) & \text{as } \|x\| \rightarrow \infty. \end{cases} \quad (17)$$

Note that (17) has a unique solution in $W_0^1(\Omega)$ if and only if the compatibility condition:

$$\int_{\Gamma} \varkappa \bar{p} ds = 0, \quad (18)$$

is satisfied.

The approach proposed here to deal with (15) is the following: determine the electric current density j_0 and the constant c that minimize the shape functional (16). We note that the minimum of the shape functional (23) is attained when $\phi \equiv 0$ on Γ . This means that in this situation, from the well-posedness of both problems (5) and (17), we have $\phi \equiv \varphi$ in Ω .

In a first step we can eliminate the variable c of the optimization problem, defining it as the global minimum $c^*(j_0)$ of (16) for any fixed j_0 , i.e., we take $c = c^*(j_0) = \arg \min_c J(\phi(j_0, c))$. In fact, $\phi = \zeta + c$, where ζ is the unique solution in $W_0^1(\Omega)$ to the following problem

$$\begin{cases} -\Delta\zeta = \mu_0 j_0 & \text{in } \Omega, \\ \frac{\partial\zeta}{\partial n} = \varkappa \bar{p} & \text{on } \Gamma, \\ \zeta(x) = o(1) & \text{as } \|x\| \rightarrow \infty. \end{cases} \quad (19)$$

From (16), and denoting $|\Gamma| = \int_{\Gamma} ds$, we have $J(\phi) = J(\zeta) + c \int_{\Gamma} \zeta ds + \frac{1}{2}c^2|\Gamma|$. Differentiating this expression with respect to c , we obtain the global minimum

$$c^*(j_0) = -|\Gamma|^{-1} \int_{\Gamma} \zeta ds. \quad (20)$$

Note also that $c = c^*(j_0)$ if and only if the integral of ϕ on Γ vanishes. In fact, taking $c = c^*(j_0)$ we have $\int_{\Gamma} \phi ds = \int_{\Gamma} \zeta ds + c^*(j_0)|\Gamma| = 0$. Conversely, if we ask for the integral of ϕ on Γ to be zero, we have $\int_{\Gamma} \zeta ds + c|\Gamma| = 0$, that has the solution $c = c^*(j_0)$.

Hence, we can formulate an equivalent optimization problem as follows: minimize the shape functional (16), where ϕ depends implicitly on j_0 only, by solving the following problem

$$\begin{cases} -\Delta\phi = \mu_0 j_0 & \text{in } \Omega, \\ \frac{\partial\phi}{\partial n} = \varkappa \bar{p} & \text{on } \Gamma, \\ \int_{\Gamma} \phi ds = 0. \end{cases} \quad (21)$$

The variational formulation of (21) is

$$\phi \in U : \int_{\Omega} \nabla\phi \cdot \nabla\eta dx = \int_{\Gamma} \varkappa \bar{p} \eta ds + \int_{\Omega} \mu_0 j_0 \eta dx \quad \forall \eta \in U, \quad (22)$$

where U is the closed subspace of $W_0^1(\Omega)$ defined as $U = \{u \in W_0^1(\Omega) : \int_{\Gamma} u ds = 0\}$.

Therefore, the proposed approach is to solve the optimization problem

$$\min_{j_0} \frac{1}{2} \|\phi\|_{L^2(\Gamma)}^2, \quad (23)$$

subject to the constraint given by (22).

Before continue, let us introduce an adjoint state v for further simplification, which is solution to the following boundary-value problem

$$\begin{cases} -\Delta v = 0 & \text{in } \Omega, \\ \frac{\partial v}{\partial n} = -\phi & \text{on } \Gamma, \\ \int_{\Gamma} v ds = 0. \end{cases} \quad (24)$$

or, equivalently, solution to the variational problem

$$v \in U : \int_{\Omega} \nabla v \cdot \nabla \eta \, dx + \int_{\Gamma} \phi \eta \, ds = 0 \quad \forall \eta \in U. \quad (25)$$

Note that the compatibility condition for (24) is satisfied, since the integral of ϕ on Γ vanishes. Hence (24) and (25) always have a unique solution. In addition, we can also split the solution $v = w + \beta$, where w is the unique solution in $W_0^1(\Omega)$ to the following problem

$$\begin{cases} -\Delta w = 0 & \text{in } \Omega, \\ \frac{\partial w}{\partial n} = -\phi & \text{on } \Gamma, \\ w(x) = o(1) & \text{as } \|x\| \rightarrow \infty, \end{cases} \quad (26)$$

and the constant $\beta = -|\Gamma|^{-1} \int_{\Gamma} w \, ds$.

4.2. The topological derivative calculation

Associated to ϕ we define the function ϕ_{ε} solution to the perturbed variational problem. In this context, the perturbation is characterized by changing the electric current distribution j_0 by a new one j_{ε} which is identical to j_0 everywhere in Ω except in two small regions $B_{\varepsilon}(x^+) \subset \Omega$ and $B_{\varepsilon}(x^-) \subset \Omega$, such that $B_{\varepsilon}(x^-) \cap B_{\varepsilon}(x^+) = \emptyset$. More precisely, j_{ε} is given by

$$j_{\varepsilon} = j_0 + I\chi_{B_{\varepsilon}(x^+)} - I\chi_{B_{\varepsilon}(x^-)}. \quad (27)$$

Therefore, the perturbed electric current distribution j_{ε} also satisfies the compatibility condition, namely

$$\int_{\Omega} j_{\varepsilon} \, dx = 0. \quad (28)$$

In this way, the shape functional associated to the perturbed problem reads:

$$\psi(\varepsilon) = J(\phi_{\varepsilon}) = \frac{1}{2} \int_{\Gamma} |\phi_{\varepsilon}|^2 \, ds, \quad (29)$$

where ϕ_{ε} is solution to the following variational problem:

$$\phi_{\varepsilon} \in U : \int_{\Omega} \nabla \phi_{\varepsilon} \cdot \nabla \eta \, dx = \int_{\Gamma} \kappa \bar{p} \eta \, ds + \int_{\Omega} \mu_0 j_{\varepsilon} \eta \, dx \quad \forall \eta \in U. \quad (30)$$

Before proceeding, let us introduce the adjoint state v_ε associated to the perturbed problem, which is solution to the variational problem

$$v_\varepsilon \in U : \int_{\Omega} \nabla v_\varepsilon \cdot \nabla \eta \, dx + \int_{\Gamma} \phi_\varepsilon \eta \, ds = 0 \quad \forall \eta \in U. \quad (31)$$

Lemma 1. *Let ϕ and ϕ_ε be the solutions to the variational problems (22) and (30), respectively. Then, there exist a constant C independent of ε such that the inequality*

$$\|\phi_\varepsilon - \phi\|_{W_0^1(\Omega)} \leq C\varepsilon, \quad (32)$$

is satisfied for any small parameter ε .

Proof. We have seen that $\phi = \zeta + c$ with ζ solution to (19) or, equivalently, solution to the variational problem

$$\zeta \in V : \int_{\Omega} \nabla \zeta \cdot \nabla \eta \, dx = \int_{\Gamma} \kappa \bar{p} \eta \, ds + \int_{\Omega} \mu_0 j_0 \eta \, dx \quad \forall \eta \in V, \quad (33)$$

where $V = \{u \in W_0^1(\Omega) : u(x) \rightarrow 0 \text{ as } \|x\| \rightarrow \infty\}$ and the constant $c = -|\Gamma|^{-1} \int_{\Gamma} \zeta \, ds$. Analogously, $\phi_\varepsilon = \zeta_\varepsilon + c_\varepsilon$ with ζ_ε solution to the variational problem

$$\zeta_\varepsilon \in V : \int_{\Omega} \nabla \zeta_\varepsilon \cdot \nabla \eta \, dx = \int_{\Gamma} \kappa \bar{p} \eta \, ds + \int_{\Omega} \mu_0 j_\varepsilon \eta \, dx \quad \forall \eta \in V, \quad (34)$$

and with the constant $c_\varepsilon = -|\Gamma|^{-1} \int_{\Gamma} \zeta_\varepsilon \, ds$. By subtracting the variational problems (33) and (34), we get

$$\int_{\Omega} \nabla(\zeta_\varepsilon - \zeta) \cdot \nabla \eta \, dx = \mu_0 I \left(\int_{B_\varepsilon(x^+)} \eta \, dx - \int_{B_\varepsilon(x^-)} \eta \, dx \right) \quad \forall \eta \in V, \quad (35)$$

Now, by taking $\eta = \zeta_\varepsilon - \zeta$, we have

$$\int_{\Omega} \|\nabla(\zeta_\varepsilon - \zeta)\|^2 \, dx = \mu_0 I \left(\int_{B_\varepsilon(x^+)} (\zeta_\varepsilon - \zeta) \, dx - \int_{B_\varepsilon(x^-)} (\zeta_\varepsilon - \zeta) \, dx \right). \quad (36)$$

Thanks to the behavior of $(\zeta_\varepsilon - \zeta)$ at infinity, there exist a constant C_1 such that the following Poincaré type inequality holds [17]

$$\|\zeta_\varepsilon - \zeta\|_{W_0^1(\Omega)}^2 \leq C_1 \|\nabla(\zeta_\varepsilon - \zeta)\|_{L^2(\Omega)}^2, \quad (37)$$

From (36) and (37) we obtain

$$\|\zeta_\varepsilon - \zeta\|_{W_0^1(\Omega)}^2 \leq C_1 \left(\int_{B_\varepsilon(x^+)} (\zeta_\varepsilon - \zeta) dx - \int_{B_\varepsilon(x^-)} (\zeta_\varepsilon - \zeta) dx \right). \quad (38)$$

Therefore, thanks to the Cauchy-Schwarz inequality there exist a constant C_2 such that

$$\|\zeta_\varepsilon - \zeta\|_{W_0^1(\Omega)}^2 \leq C_2 \varepsilon \left(\|\zeta_\varepsilon - \zeta\|_{L^2(B_\varepsilon(x^+))} + \|\zeta_\varepsilon - \zeta\|_{L^2(B_\varepsilon(x^-))} \right). \quad (39)$$

Let $\rho(x) = [\sqrt{1 + \|x\|^2} \log(2 + \|x\|^2)]^{-1}$. Then $0 < \rho(x) < 1$ for all $x \in \Omega$. Let us introduce $\rho^* = \inf\{\rho(x), x \in B_{\varepsilon_0}(x^+) \cup B_{\varepsilon_0}(x^-)\}$ with the constant $\varepsilon_0 > 0$. Then, for any $\varepsilon < \varepsilon_0$ we have

$$\begin{aligned} \|\zeta_\varepsilon - \zeta\|_{L^2(B_\varepsilon(x^+))} &\leq \frac{1}{\rho^*} \|\rho(\zeta_\varepsilon - \zeta)\|_{L^2(B_\varepsilon(x^+))} \\ &\leq \frac{1}{\rho^*} \|\rho(\zeta_\varepsilon - \zeta)\|_{L^2(\Omega)} \\ &\leq \frac{1}{\rho^*} \|\zeta_\varepsilon - \zeta\|_{W_0^1(\Omega)}, \end{aligned} \quad (40)$$

and

$$\|\zeta_\varepsilon - \zeta\|_{L^2(B_\varepsilon(x^-))} \leq \frac{1}{\rho^*} \|\zeta_\varepsilon - \zeta\|_{W_0^1(\Omega)}. \quad (41)$$

Then, from (39), (40) and (41) there exist a constant C_3 such that

$$\|\zeta_\varepsilon - \zeta\|_{W_0^1(\Omega)}^2 \leq C_3 \varepsilon \|\zeta_\varepsilon - \zeta\|_{W_0^1(\Omega)}, \quad (42)$$

that can be expressed as

$$\|\zeta_\varepsilon - \zeta\|_{W_0^1(\Omega)} \leq C_3 \varepsilon. \quad (43)$$

On the other hand, from the Cauchy-Schwarz inequality and the trace theorem, we obtain

$$\left| \int_{\Gamma} (\zeta_\varepsilon - \zeta) ds \right| \leq C_4 |\Gamma| \|\zeta_\varepsilon - \zeta\|_{W_0^1(\Omega)}. \quad (44)$$

Therefore,

$$|c_\varepsilon - c| \leq C_4 \|\zeta_\varepsilon - \zeta\|_{W_0^1(\Omega)}. \quad (45)$$

Using (43), there exist a constant C_5 such that

$$|c_\varepsilon - c| \leq C_5 \varepsilon. \quad (46)$$

Finally,

$$\|\phi_\varepsilon - \phi\|_{W_0^1(\Omega)} \leq \|\zeta_\varepsilon - \zeta\|_{W_0^1(\Omega)} + |c_\varepsilon - c| \|1\|_{W_0^1(\Omega)}, \quad (47)$$

and using (43) and (46) we obtain (32) with $C = C_3 + C_5 \|1\|_{W_0^1(\Omega)}$. \square

Lemma 2. *Let v and v_ε be solutions the the variational problems (25) and (31), respectively. Then, we have the following estimate for the difference $v_\varepsilon - v$,*

$$\|v_\varepsilon - v\|_{W_0^1(\Omega)} \leq C \varepsilon, \quad (48)$$

where C is a constant independent of the small parameter ε .

Proof. According to (26), the solution of the adjoint problem can be obtained as $v = w + \beta$ with w solution to the following variational problem

$$w \in V : \int_{\Omega} \nabla w \cdot \nabla \eta \, dx + \int_{\Gamma} \phi \eta \, ds = 0 \quad \forall \eta \in V, \quad (49)$$

and with the constant $\beta = -|\Gamma| \int_{\Gamma} w \, ds$. Analogously, $v_\varepsilon = w_\varepsilon + \beta_\varepsilon$ with w_ε solution to the variational problem

$$w_\varepsilon \in V : \int_{\Omega} \nabla w_\varepsilon \cdot \nabla \eta \, dx + \int_{\Gamma} \phi_\varepsilon \eta \, ds = 0 \quad \forall \eta \in V, \quad (50)$$

and with the constant $\beta_\varepsilon = -|\Gamma| \int_{\Gamma} w_\varepsilon \, ds$. By subtracting the variational problems (49) and (50), we get

$$\int_{\Omega} \nabla(w_\varepsilon - w) \cdot \nabla \eta \, dx = \int_{\Gamma} (\phi_\varepsilon - \phi) \eta \, ds \quad \forall \eta \in V, \quad (51)$$

Now, by taking $\eta = w_\varepsilon - w$, we have

$$\int_{\Omega} \|\nabla(w_\varepsilon - w)\|^2 \, dx = \int_{\Gamma} (\phi_\varepsilon - \phi)(w_\varepsilon - w) \, ds. \quad (52)$$

Thanks to the behavior of $(w_\varepsilon - w)$ at infinity, the Poincaré inequality gives [17]

$$\|w_\varepsilon - w\|_{W_0^1(\Omega)}^2 \leq C_1 \|\nabla(w_\varepsilon - w)\|_{L^2(\Omega)}^2, \quad (53)$$

From (52) and (53) we obtain

$$\|w_\varepsilon - w\|_{W_0^1(\Omega)}^2 \leq C_1 \int_{\Gamma} (\phi_\varepsilon - \phi)(w_\varepsilon - w) dx. \quad (54)$$

By taking into account the Cauchy-Schwarz inequality and the trace theorem, there exist a constant C_2 such that

$$\begin{aligned} \|w_\varepsilon - w\|_{W_0^1(\Omega)}^2 &\leq C_1 \|\phi_\varepsilon - \phi\|_{H^{\frac{1}{2}}(\Gamma)} \|w_\varepsilon - w\|_{H^{\frac{1}{2}}(\Gamma)} \\ &\leq C_2 \|\phi_\varepsilon - \phi\|_{W_0^1(\Omega)} \|w_\varepsilon - w\|_{W_0^1(\Omega)}. \end{aligned} \quad (55)$$

Therefore, using Lemma 1, there exist C_3 such that

$$\|w_\varepsilon - w\|_{W_0^1(\Omega)}^2 \leq C_3 \varepsilon \|w_\varepsilon - w\|_{W_0^1(\Omega)}, \quad (56)$$

which leads to

$$\|w_\varepsilon - w\|_{W_0^1(\Omega)} \leq C_3 \varepsilon. \quad (57)$$

In addition, from the Cauchy-Schwarz inequality and the trace theorem, we obtain

$$\left| \int_{\Gamma} (w_\varepsilon - w) ds \right| \leq C_4 |\Gamma| \|w_\varepsilon - w\|_{W_0^1(\Omega)}. \quad (58)$$

Therefore,

$$|\beta_\varepsilon - \beta| \leq C_4 \|w_\varepsilon - w\|_{W_0^1(\Omega)}. \quad (59)$$

From the result (57), there exist a constant C_5 such that

$$|\beta_\varepsilon - \beta| \leq C_5 \varepsilon. \quad (60)$$

Finally,

$$\|v_\varepsilon - v\|_{W_0^1(\Omega)} \leq \|w_\varepsilon - w\|_{W_0^1(\Omega)} + |\beta_\varepsilon - \beta| \|1\|_{W_0^1(\Omega)}, \quad (61)$$

and using (57) and (60) we obtain (48) with $C = C_3 + C_5 \|1\|_{W_0^1(\Omega)}$. \square

Among the methods for calculation of the topological derivative currently available in literature, here we shall adopt the methodology developed in [52], which is given by the following result

$$D_T\psi = \lim_{\varepsilon \rightarrow 0} \frac{1}{f'(\varepsilon)} \frac{d}{d\varepsilon} \psi(\varepsilon), \quad (62)$$

where $\frac{d}{d\varepsilon} \psi(\varepsilon)$ is the derivative of $\psi(\varepsilon)$ with respect to the small parameter ε , which can be seen as the sensitivity of $\psi(\varepsilon)$, in the classical sense [53, 54] to the domain perturbation produced by an uniform expansion of the perturbation B_ε . Therefore, we can use the concept of shape sensitivity analysis as an intermediate step in the topological derivative calculation. This procedure enormously simplifies the analysis, allowing us to state the following result:

Theorem 3. *The topological derivative of the shape functional (15) is*

$$D_T\psi = -\mu_0 I (v(x^+) - v(x^-)) . \quad (63)$$

Therefore, the topological asymptotic expansion of the shape functional reads

$$\psi(\varepsilon) = \psi(0) - \pi \varepsilon^2 \mu_0 I (v(x^+) - v(x^-)) + o(\varepsilon^2) . \quad (64)$$

Proof. The shape derivative of the functional (29) can be obtained as follows

$$\frac{d}{d\varepsilon} \psi(\varepsilon) = \dot{J}(\phi_\varepsilon) = \int_{\Gamma} \phi_\varepsilon \dot{\phi}_\varepsilon ds . \quad (65)$$

Now, let us calculate the shape derivative of the state equation, which leads to

$$\dot{\phi}_\varepsilon \in U : \int_{\Omega} \nabla \dot{\phi}_\varepsilon \cdot \nabla \eta dx = \frac{2}{\varepsilon} \mu_0 I \left(\int_{B_\varepsilon(x^+)} \eta dx - \int_{B_\varepsilon(x^-)} \eta dx \right) \quad \forall \eta \in U . \quad (66)$$

Since $\dot{\phi}_\varepsilon \in U$, we can take it as a test function in (31), namely $\eta = \dot{\phi}_\varepsilon$, to obtain

$$\int_{\Omega} \nabla v_\varepsilon \cdot \nabla \dot{\phi}_\varepsilon dx = - \int_{\Gamma} \phi_\varepsilon \dot{\phi}_\varepsilon ds . \quad (67)$$

In the same way, since $v_\varepsilon \in U$, we can take it as a test function in (30), namely $\eta = v_\varepsilon$, to obtain

$$\int_{\Omega} \nabla \dot{\phi}_\varepsilon \cdot \nabla v_\varepsilon \, dx = \frac{2}{\varepsilon} \mu_0 I \left(\int_{B_\varepsilon(x^+)} v_\varepsilon \, dx - \int_{B_\varepsilon(x^-)} v_\varepsilon \, dx \right). \quad (68)$$

By comparing both equations and taking into account the symmetry of the bilinear forms on their left-hand sides, we have from (65) the following important result

$$\dot{J}(\phi_\varepsilon) = -\frac{2}{\varepsilon} \mu_0 I \left(\int_{B_\varepsilon(x^+)} v_\varepsilon \, dx - \int_{B_\varepsilon(x^-)} v_\varepsilon \, dx \right). \quad (69)$$

In addition, by Lemma 2 we have

$$\|v_\varepsilon - v\|_{W_0^1(\Omega)} \leq C \varepsilon. \quad (70)$$

Therefore we can approximate v_ε as

$$v_\varepsilon(x) = v(x) + O(\varepsilon). \quad (71)$$

Then, from the regularity of v_ε and v at x^+ and x^- we also have

$$v_\varepsilon(x^+) = v(x^+) + O(\varepsilon) \quad \text{and} \quad v_\varepsilon(x^-) = v(x^-) + O(\varepsilon), \quad (72)$$

where v is solution to (25). From these elements, we obtain

$$\begin{aligned} \frac{d}{d\varepsilon} \psi(\varepsilon) &= \dot{J}(\phi_\varepsilon) = -\frac{2}{\varepsilon} \mu_0 I \left(\pi \varepsilon^2 v(x^+) - \pi \varepsilon^2 v(x^-) \right) + O(\varepsilon^2) \\ &= -2\pi \varepsilon \mu_0 I \left(v(x^+) - v(x^-) \right) + O(\varepsilon^2). \end{aligned} \quad (73)$$

From the result (62) we obtain

$$D_T \psi = -\lim_{\varepsilon \rightarrow 0} \frac{2\pi \varepsilon}{f'(\varepsilon)} \mu_0 I \left(v(x^+) - v(x^-) + O(\varepsilon) \right). \quad (74)$$

Therefore, in order to extract the main term of the above expansion, we can choose $f'(\varepsilon) = 2\pi \varepsilon$ ($f(\varepsilon) = \pi \varepsilon^2$) and calculate the limit passage $\varepsilon \rightarrow 0$ to obtain the desired result. \square

Since we want to minimize the shape functional ψ , in the numerical approach we have to include a pair of inductors at the points x^+ (positive inductor) and x^- (negative inductor) where the topological derivative $D_T \psi$ takes its more negative values.

5. Numerical Method

5.1. The exterior Neumann problem

We have seen that to compute the topological derivative given by formula (63) we have to solve the Neumann problems (21) and (24). To obtain approximate solutions for these problems, we can resort again to functions ζ and w , solutions to (19) and (26), respectively. So, let us consider the following general form of the exterior Neumann problem:

$$\begin{cases} -\Delta u = b & \text{in } \Omega, \\ \frac{\partial u}{\partial n} = q & \text{on } \Gamma, \\ u(x) = o(1) & \text{as } \|x\| \rightarrow \infty, \end{cases} \quad (75)$$

The solution u of (75) satisfies the following integral equation [18, 55, 56, 57]

$$c(\xi)u(\xi) + \int_{\Gamma} q^*(\xi, x)u \, d\gamma - \int_{\Gamma} u^*(\xi, x)q(x) \, d\gamma = \int_{\Omega} u^*(\xi, x)b(x) \, dx, \quad (76)$$

where u^* is the fundamental solution of the problem, $u^*(\xi, x) = -\frac{1}{2\pi} \log \|\xi - x\|$, $q^*(\xi, x) = \frac{\partial u^*}{\partial n}(\xi, x)$, the characteristic function $c(\xi) = 1$, for any interior point ξ , and $c(\xi) = \frac{\Delta\theta}{2\pi}$, for any point $\xi \in \Gamma$, where $\Delta\theta$ is the angle, internal to Ω , formed by the right and left tangents to Γ at ξ ($c(\xi) = \frac{1}{2}$ at points where Γ is smooth). The first integral on left hand side of (76) must be understood in the Cauchy principal value sense.

The spatial discretization consists in approximating the boundary Γ into N linear elements Γ_j , $1 \leq j \leq N$. The functions u and q are approximated inside each element by piecewise linear polynomials in the form:

$$u(x) = \mathbf{N}(x)\mathbf{u}^{(j)}, \quad q(x) = \mathbf{N}(x)\mathbf{q}^{(j)}, \quad \text{in } \Gamma_j, \quad (77)$$

where \mathbf{N} is the 1×2 matrix of the linear interpolation functions and $\mathbf{u}^{(j)}$ and $\mathbf{q}^{(j)}$ are the vectors that contain the nodal variables corresponding to u and q in the element Γ_j . The collocation boundary element method (BEM), builds a linear system imposing (76) at each node ξ_i of the boundary:

$$c_i u_i + \sum_{j=1}^N \mathbf{h}_{ij} \mathbf{u}^{(j)} - \sum_{j=1}^N \mathbf{g}_{ij} \mathbf{q}^{(j)} = u_1(\xi_i), \quad 1 \leq i \leq N, \quad (78)$$

where the element matrices \mathbf{h}_{ij} and \mathbf{g}_{ij} are:

$$\mathbf{h}_{ij} = \int_{\Gamma_j} q^*(\xi, x) \mathbf{N}(x) d\gamma, \quad \mathbf{g}_{ij} = \int_{\Gamma_j} u^*(\xi, x) \mathbf{N}(x) d\gamma, \quad (79)$$

and the function u_1 , which is a particular solution of (75), is defined as:

$$u_1(\xi) = \int_{\Omega} u^*(\xi, x) b(x) dx. \quad (80)$$

The linear system (78) can be expressed in matrix form as:

$$\mathbf{H}\mathbf{u} = \mathbf{G}\mathbf{q} + \mathbf{u}_1, \quad (81)$$

where \mathbf{H} was assembled from the values of c_i and \mathbf{h}_{ij} , \mathbf{G} from the values of matrices \mathbf{g}_{ij} , the vectors \mathbf{u} and \mathbf{q} contain all the nodal variables corresponding to u and q , respectively, and $(\mathbf{u}_1)_i = u_1(\xi_i)$.

Once solved the linear system (81), the solution \mathbf{u} provides the piecewise approximation of u on Γ by using (77). The approximate solution at interior points is obtained using (76), with $c(\xi) = 1$, and with u and q defined on Γ by the interpolation expressions of (77).

5.2. Construction of the solution

Before starting with the optimization process, we have to define a mesh of linear elements approximating the boundary Γ , and a mesh of cells in a region inside Ω surrounding the liquid metal. For each of these cells we set the initial value for the parameters α_p of (11). The solution of the design problem will be obtained changing the values of α_p . **For academic examples, we compute the constant value p_0 using (13), in real life cases p_0 is a given data.** For numerical calculations, the curvature \mathcal{C} at a node of the boundary mesh is approximated by the curvature of the circumference defined by it and adjacent nodes. Inside the elements the curvature is linearly interpolated. Next we define the function $\varkappa = \pm 1$ with a sign change at each global maximum of the piecewise approximation of the curvature. Curves for which this definition of \varkappa does not satisfies the compatibility condition (18), or having an odd number of global maximum points, are strictly not shapable. Finally, we assign a power of two to the integer variable NC.

The procedure proposed here to build the solution is the following:

1. Find ϕ and v on the boundary solving the Neumann exterior problems (17) and (24) and compute the initial value of the objective function $J(\phi)$.
2. Compute the adjoint state v value at the center of each cell of the mesh.
3. For the set of cells with $\alpha_p \leq 0$, set $\alpha_p := \alpha_p + 1$ to the NC cells that have the largest values of v . For the set of cells with $\alpha_p \geq 0$, set $\alpha_p := \alpha_p - 1$ to the NC cells that have the smallest values of v .
4. Solve the Neumann exterior problems (17) and (24) on the boundary and compute the new value of the objective function $J(\phi)$. If the objective function has decreased then return to step (2). Otherwise, undo the changes made in step (3) and set $NC := NC/2$. If $NC < 1$ stop. Otherwise, return to step (3).

Note that the previous procedure generates a sequence of solutions that monotonically decrease the value of the objective function. Note also that the stopping criterium is the most rigorous possible, because the procedure stops only if it can not find other solution having a smaller value of the objective function.

Step (2) is by far the most expensive of the previous procedure. Roughly speaking, the number of operations of this step is proportional to the number of elements of the boundary mesh times the number of cells of the domain mesh. The number of operations of steps (1) and (4) is related only to the number of elements of the boundary mesh. The number of operations of step (3) is also related to the number of cells of the domain mesh, but the ordering operations of this step can be performed in significantly less time than the operations of step (2).

6. Numerical examples

6.1. Example 1

The target shape of this example is the solution of a direct free-surface problem for a liquid metal column of cross-section area $S_0 = \pi$, considering four distributed currents of density $I = 0.5$ as shown in Fig. 1. The surface tension $\sigma = 1.0 \times 10^{-4}$ and $\mu_0 = 1.0$. For the inverse problem we consider two cases, named Ex1a and Ex1b, for meshes of cells of size $D = 0.05$ and $D = 0.02$ respectively, defined in the region shown in Fig. 1. The results

obtained are shown in Fig. 2. The evolution of the objective function along the iterative process is shown in Fig. 3.

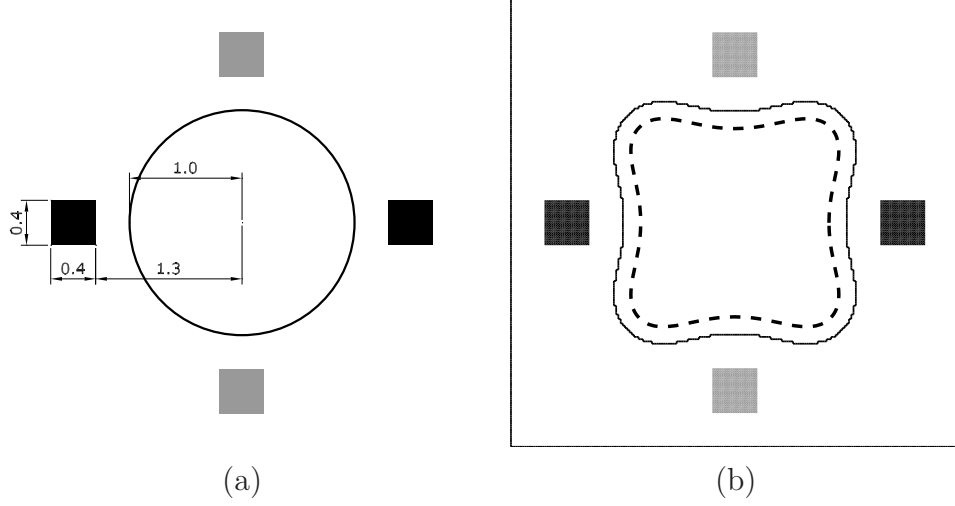


Figure 1: Example 1. (a) Initial configuration of the direct free-surface problem. (b) Target shape and exact solution. Black area: positive inductors, gray area: negative inductors, dashed line: target shape, thin solid line: boundary of the mesh of cells.

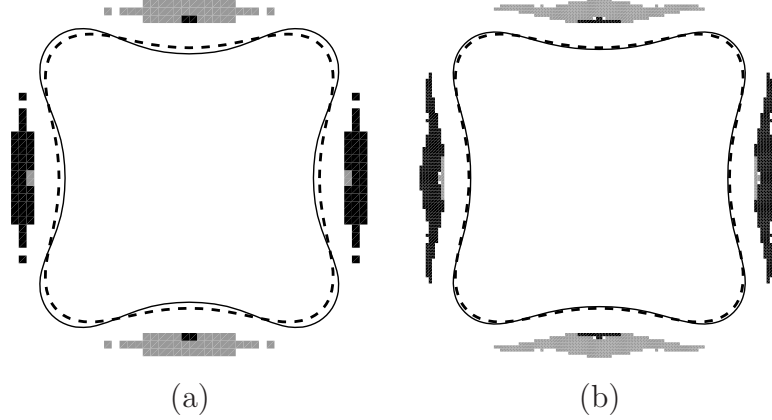


Figure 2: Example 1. (a) Solution for a mesh of cells of size $D = 0.05$. (b) Solution for a mesh of cells of size $D = 0.02$. Black area: positive inductors, gray area: negative inductors, dashed line: target shape, thin solid line: equilibrium shape.

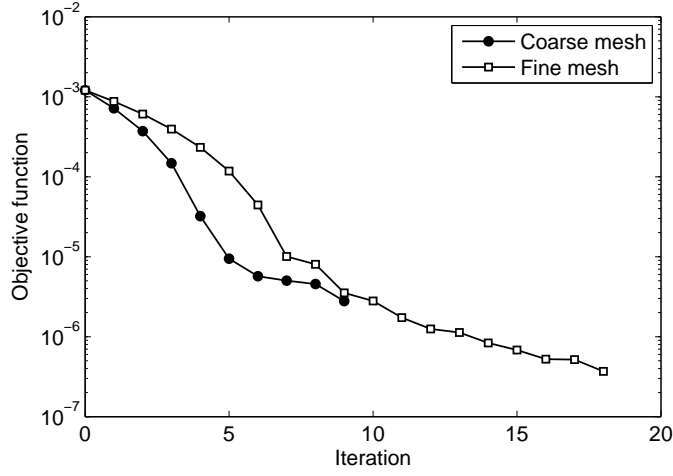


Figure 3: Example 1. Evolution of the objective function.

6.2. Example 2

This example is similar to the previous one, with the only difference that the distributed currents were defined for a density $I = 0.8$. Figure 4 shows the target shape in this case. As in the previous example, two cases are considered, named Ex2a and Ex2b, for meshes of cells of size $D = 0.05$ and $D = 0.02$ respectively, defined in the region shown in Fig. 4. The results obtained are shown in Fig. 5. The evolution of the objective function along the iterative process is shown in Fig. 6.

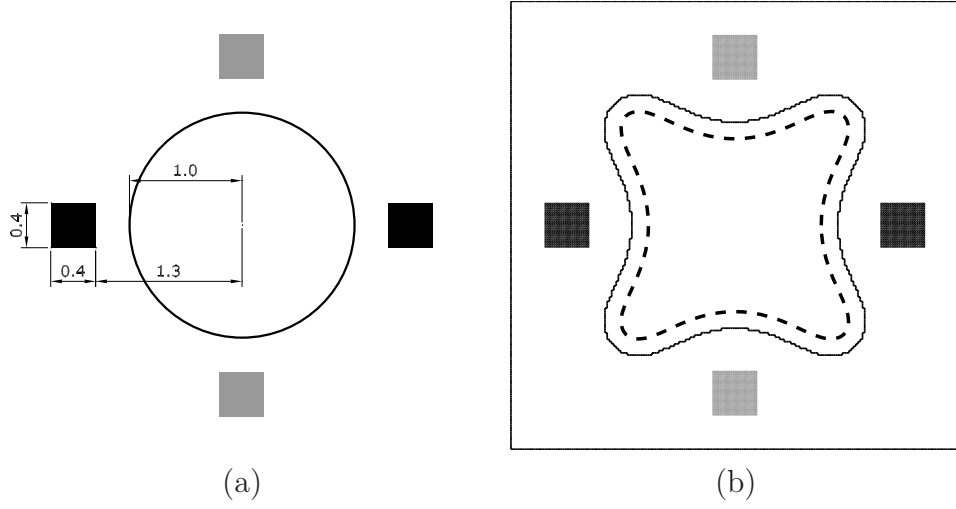


Figure 4: Example 2. (a) Initial configuration of the direct free-surface problem. (b) Target shape and exact solution. Black area: positive inductors, gray area: negative inductors, dashed line: target shape, thin solid line: boundary of the mesh of cells.

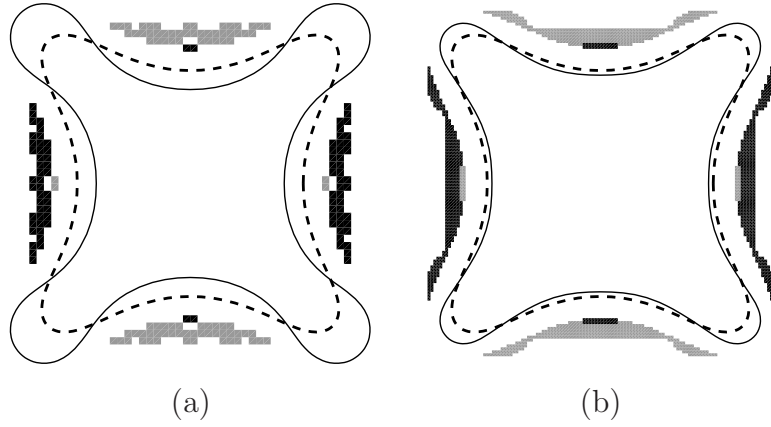


Figure 5: Example 2. (a) Solution for a mesh of cells of size $D = 0.05$. (b) Solution for a mesh of cells of size $D = 0.02$. Black area: positive inductors, gray area: negative inductors, dashed line: target shape, thin solid line: equilibrium shape.

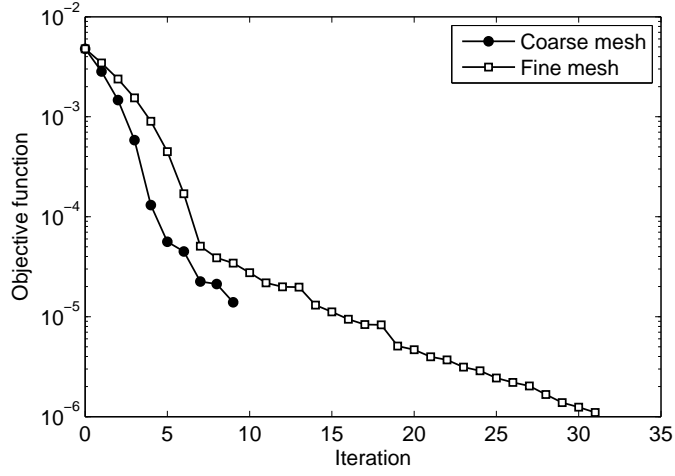


Figure 6: Example 2. Evolution of the objective function.

6.3. Example 3

In this case, six distributed currents of density $I = 0.4$ are considered as shown in Fig. 7. For the inverse problem we consider two cases, named Ex1a and Ex1b, for meshes of cells of size $D = 0.05$ and $D = 0.02$ respectively, defined in the region shown in Fig. 7. The results obtained are shown in Fig. 8. The evolution of the objective function along the iterative process is shown in Fig. 9.

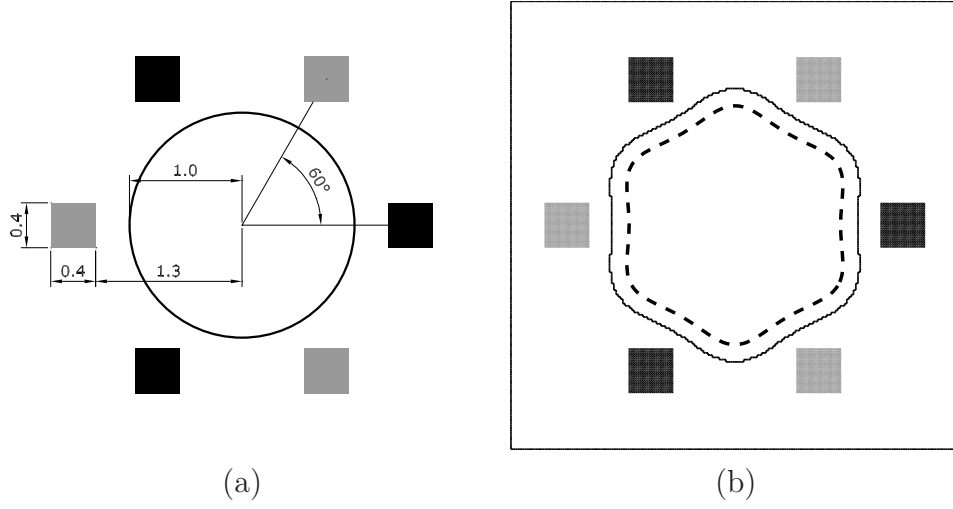


Figure 7: Example 3. (a) Initial configuration of the direct free-surface problem. (b) Target shape and exact solution. Black area: positive inductors, gray area: negative inductors, dashed line: target shape, thin solid line: boundary of the mesh of cells.

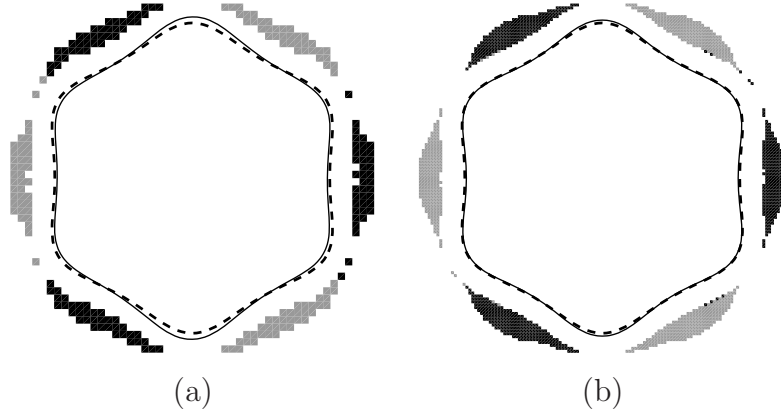


Figure 8: Example 3. (a) Solution for a mesh of cells of size $D = 0.05$. (b) Solution for a mesh of cells of size $D = 0.02$. Black area: positive inductors, gray area: negative inductors, dashed line: target shape, thin solid line: equilibrium shape.

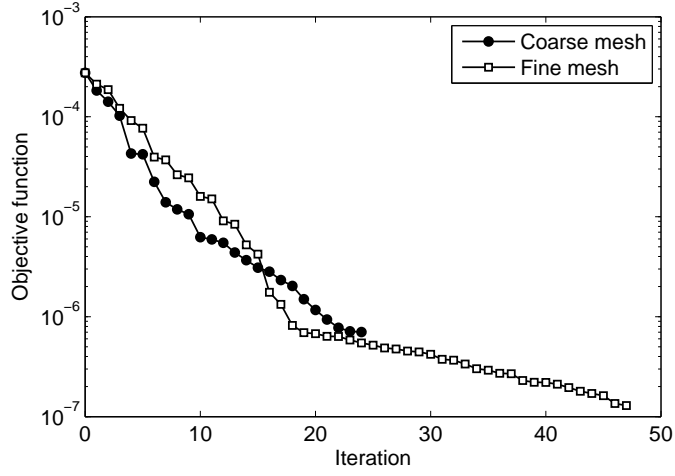


Figure 9: Example 3. Evolution of the objective function.

6.4. Example 4

This example is similar to the previous one, with the only difference that the distributed currents were defined for a density $I = 0.8$. Figure 10 shows the target shape in this case. For the inverse problem we consider two cases, named Ex4a and Ex4b, for meshes of cells of size $D = 0.05$ and $D = 0.02$ respectively, defined in the region shown in Fig. 10. The results obtained are shown in Fig. 11. The evolution of the objective function along the iterative process is shown in Fig. 12.

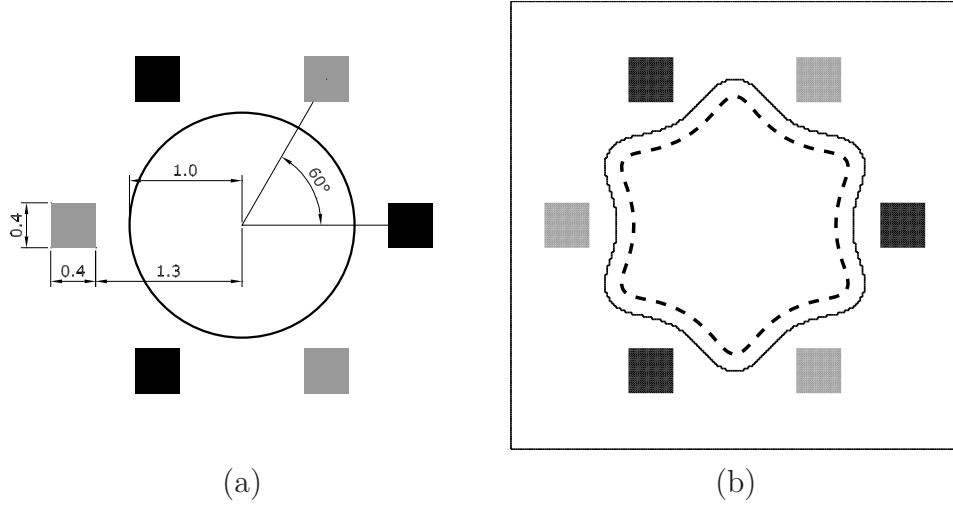


Figure 10: Example 4. (a) Initial configuration of the direct free-surface problem. (b) Target shape and exact solution. Black area: positive inductors, gray area: negative inductors, dashed line: target shape, thin solid line: boundary of the mesh of cells.

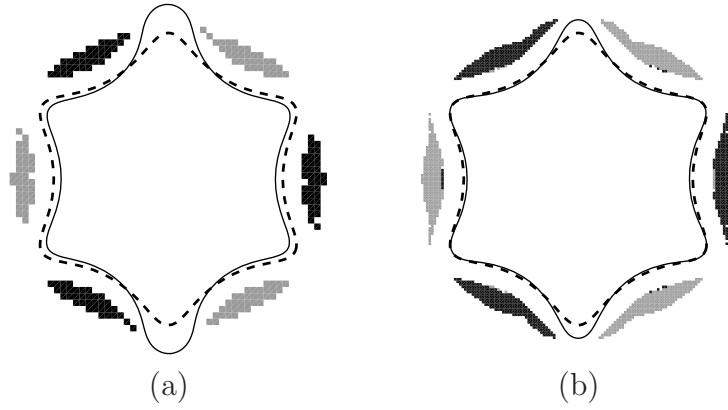


Figure 11: Example 4. (a) Solution for a mesh of cells of size $D = 0.05$. (b) Solution for a mesh of cells of size $D = 0.02$. Black area: positive inductors, gray area: negative inductors, dashed line: target shape, thin solid line: equilibrium shape.

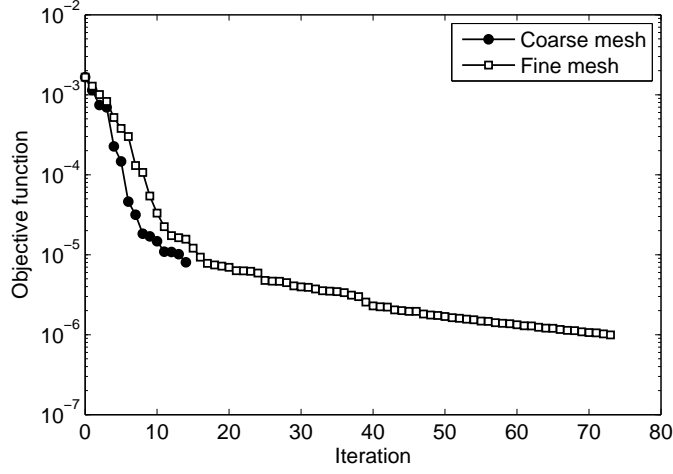


Figure 12: Example 4. Evolution of the objective function.

6.5. Example 5

The target shape of this example is the round rectangle depicted in Fig. 13. The current density $I = 0.2$, $\sigma = 1.0 \times 10^{-4}$ and $\mu_0 = 1.0$. We consider two cases, named Ex5a and Ex5b, for meshes of cells of size $D = 0.05$ and $D = 0.02$ respectively, defined in the region shown in Fig. 13. Two fictitious points of maximum curvature were defined in this example with the purpose of satisfying the compatibility equation. The results obtained are shown in Fig. 14. The evolution of the objective function along the iterative process is shown in Fig. 15.

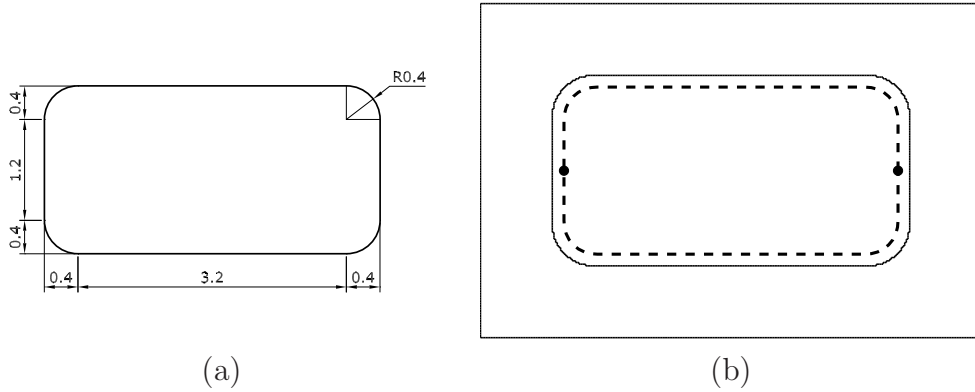


Figure 13: Example 5. (a) Description of the problem geometry. (b) Target shape. Dashed line: target shape, thin solid line: boundary of the mesh of cells, black dots: fictitious points of maximum curvature.

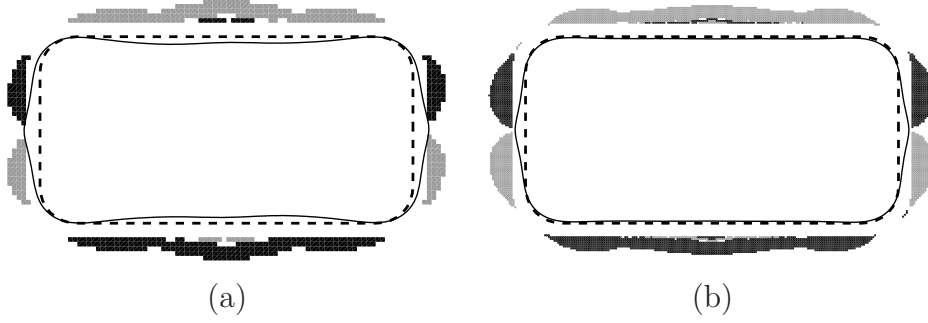


Figure 14: Example 5. (a) Solution for a mesh of cells of size $D = 0.05$. (b) Solution for a mesh of cells of size $D = 0.02$. Black area: positive inductors, gray area: negative inductors, dashed line: target shape, thin solid line: equilibrium shape.

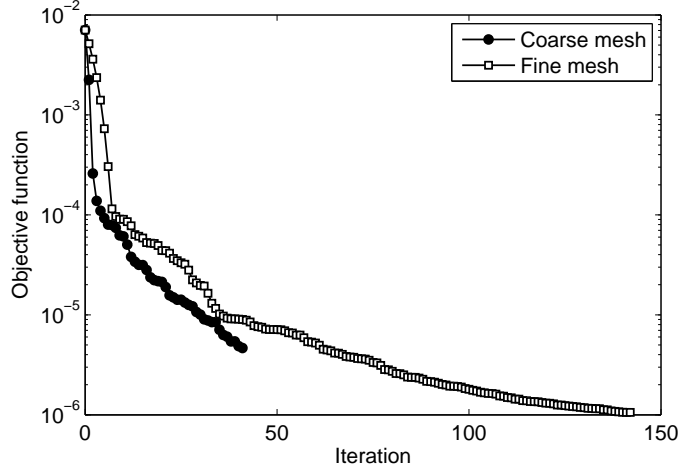


Figure 15: Example 5. Evolution of the objective function.

6.6. Example 6

The target shape of this example is depicted in Fig. 16. The current density $I = 0.2$, $\sigma = 1.0 \times 10^{-4}$ and $\mu_0 = 1.0$. We consider two cases, named Ex6a and Ex6b, for meshes of cells of size $D = 0.05$ and $D = 0.02$ respectively, defined in the region shown in Fig. 16. The results obtained are shown in Fig. 17. The evolution of the objective function along the iterative process is shown in Fig. 18.

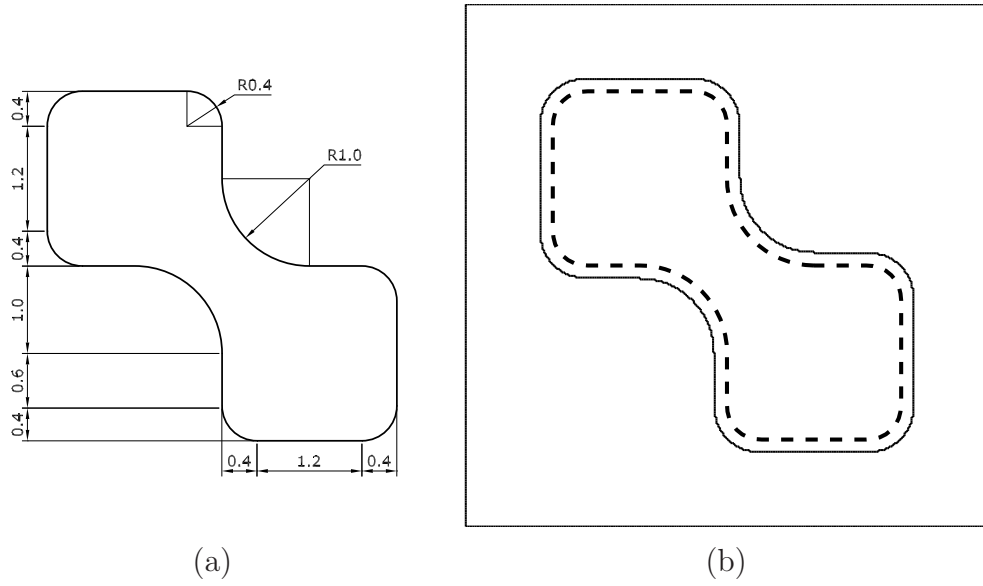


Figure 16: Example 6. (a) Description of the problem geometry. (b) Target shape. Dashed line: target shape, thin solid line: boundary of the mesh of cells.

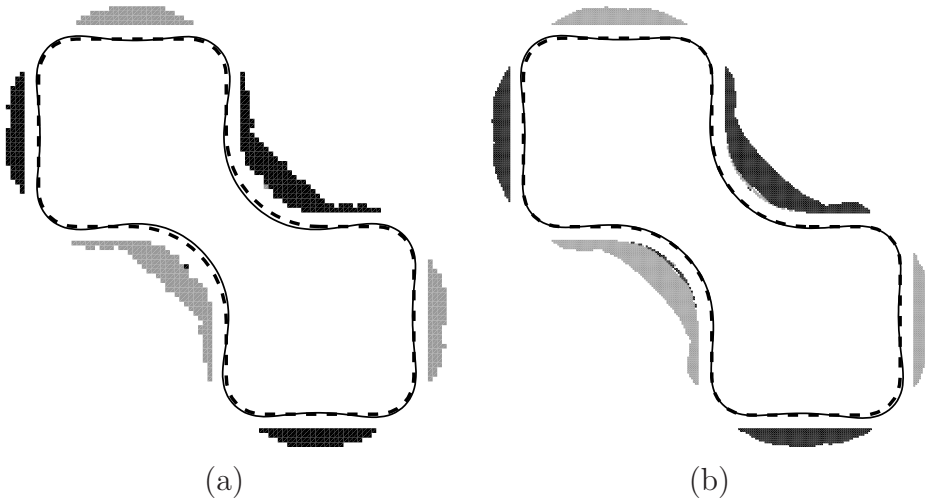


Figure 17: Example 6. (a) Solution for a mesh of cells of size $D = 0.05$. (b) Solution for a mesh of cells of size $D = 0.02$. Black area: positive inductors, gray area: negative inductors, dashed line: target shape, thin solid line: equilibrium shape.

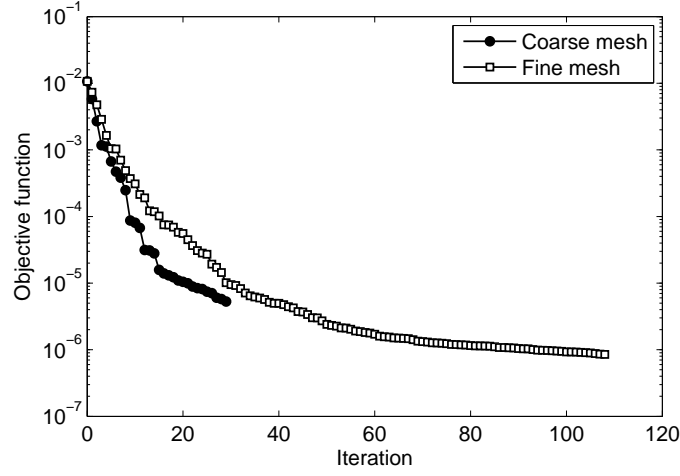


Figure 18: Example 6. Evolution of the objective function.

6.7. Example 7

The target shape of this example is depicted in Fig. 19. The current density $I = 0.2$, $\sigma = 1.0 \times 10^{-4}$ and $\mu_0 = 1.0$. We consider two cases, named Ex7a and Ex7b, for meshes of cells of size $D = 0.05$ and $D = 0.02$ respectively, defined in the region shown in Fig. 19. Two fictitious points of maximum curvature were defined in this example with the purpose of satisfying the compatibility equation. The results obtained are shown in Fig. 20. The evolution of the objective function along the iterative process is shown in Fig. 21.

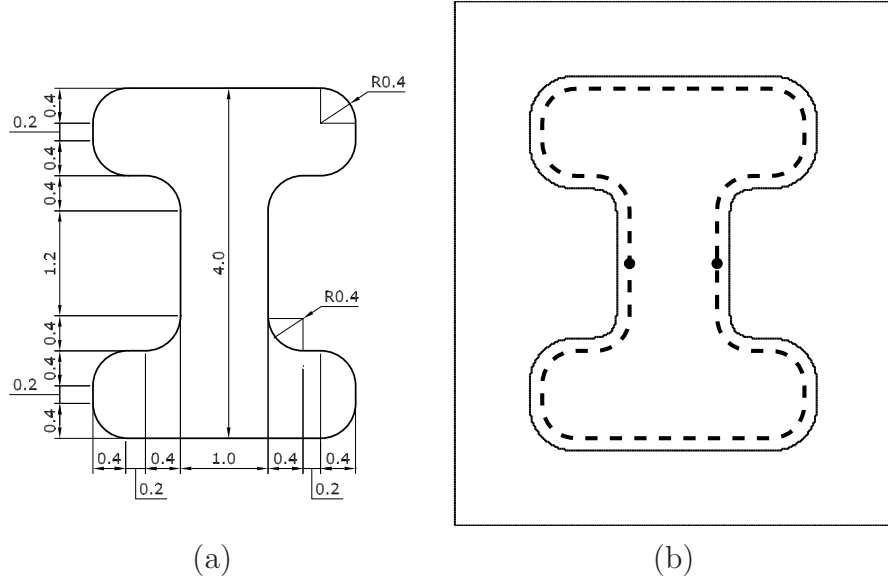


Figure 19: Example 7. (a) Description of the problem geometry. (b) Target shape. Dashed line: target shape, thin solid line: boundary of the mesh of cells, black dots: fictitious points of maximum curvature.

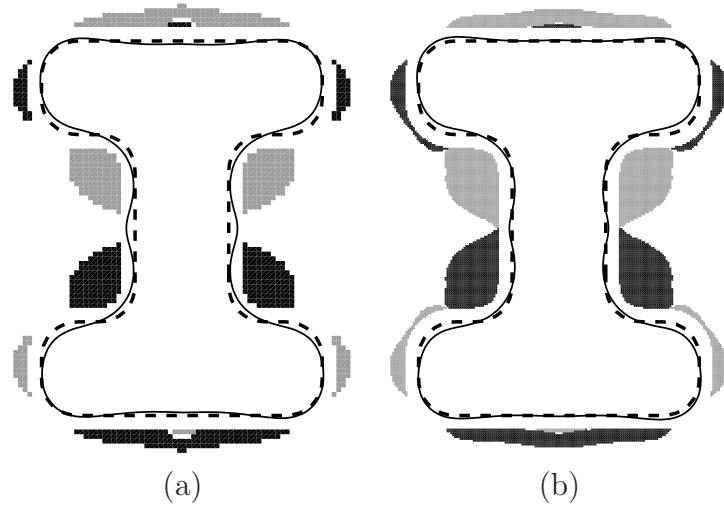


Figure 20: Example 7. (a) Solution for a mesh of cells of size $D = 0.05$. (b) Solution for a mesh of cells of size $D = 0.02$. Black area: positive inductors, gray area: negative inductors, dashed line: target shape, thin solid line: equilibrium shape.

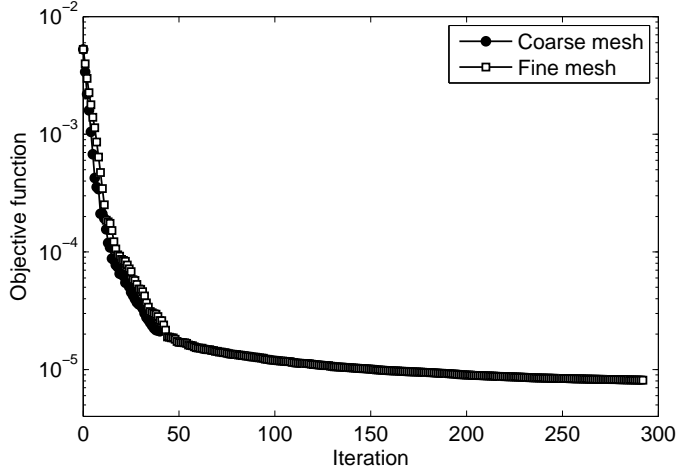


Figure 21: Example 7. Evolution of the objective function.

6.8. Results summary

Table 1 resumes the information about the considered examples. For each one the number of iterations performed by the optimization algorithm is indicated as well as the final value of the objective function. Note that the target shapes of examples 1 to 4 are solutions of direct free-surface problems considering known electric currents. Then, those currents constitute exact solutions for the inverse problem considered here. However, as the figures above shown, the inductors obtained by the optimization algorithm are clearly different from the known exact solutions. This fact, instead of indicating that the algorithm did not work properly, suggests that the inductor design problem have multiple solutions. Table 1 shows that, for all these examples, the optimization algorithm obtained approximated solutions with a clearly lower value of the total intensity of current than the associated to the known exact solutions. Thus, the results obtained suggest the idea that the optimization algorithm looks for an economic design, which is consistent with the idea that inspires the use of the topological derivative: the algorithm puts inductors in the location where they produce the largest influence on the shape functional.

Examples 5 to 7 show that the proposed approach is also effective dealing with truly inverse problems defined considering general shapes. The best result was obtained for the Example 6, which, because of the symmetry of the problem, exactly satisfies the compatibility equation (18). The examples

5 and 7 required the definition of fictitious points of maximum curvature to satisfy the compatibility equation. For these examples, the results of the free-surface problem show that the equilibrium shapes have points of maximum curvature in places where they should not be. The equilibrium shapes obtained for these examples are, however, quite close to the target shapes.

Table 1: Results summary.

Example	NE	TC	NC	Iter	II	IS	IOF	FOF
Ex1a	128	4692	16	9	0.160	0.110	1.209e-03	2.779e-06
Ex1b	128	29304	64	18	0.160	0.118	1.209e-03	3.681e-07
Ex2a	184	4624	16	9	0.256	0.176	4.773e-03	1.394e-05
Ex2b	184	28912	64	31	0.256	0.204	4.773e-03	1.103e-06
Ex3a	120	4724	16	24	0.192	0.112	2.747e-04	7.013e-07
Ex3b	120	29520	64	47	0.192	0.109	2.747e-04	1.292e-07
Ex4a	228	4688	16	14	0.384	0.208	1.663e-03	8.026e-06
Ex4b	228	29288	64	73	0.384	0.229	1.663e-03	9.936e-07
Ex5a	120	5744	32	42	–	0.143	7.059e-03	4.691e-06
Ex5b	120	36128	128	142	–	0.160	7.059e-03	1.056e-06
Ex6a	152	10228	32	29	–	0.161	1.066e-02	5.300e-06
Ex6b	152	64120	128	108	–	0.173	1.066e-02	8.523e-07
Ex7a	180	7864	32	40	–	0.216	5.258e-03	2.113e-05
Ex7b	180	49368	128	292	–	0.264	5.258e-03	8.129e-06

NE: number of elements, TC: total number of cells, NC: initial number of cells that are selected to change the sign, Iter: number of iterations performed, II: total intensity of the positive inductors of the known exact solution. IS: total intensity of the positive inductors of the solution obtained, IOF: initial value of the objective function, FOF: final value of the objective function.

7. Conclusions

In this paper we have described a new method for the topology design of inductors in electromagnetic casting. For the two-dimensional case, a new formulation of the design problem based on the Kohn-Vogelius functional was stated. The topological derivative of the Kohn-Vogelius functional regarding

the introduction of small inductors was derived. A numerical procedure that makes use of the topological derivative to construct the solution was proposed.

Some examples presented show that the method proposed is effective to design suitable inductors. For some examples with known exact solutions, the method was able to obtain solutions with a clearly lower value of the total intensity of current than that associated to the known solution. This fact suggests that the use of topological derivatives gives the method the intrinsic ability to choose an economical design among those belonging to the set of solutions. Some other examples with unknown solutions were also successfully resolved.

In summary, the method proposed is easy to code and can be successfully used in the design of inductors in electromagnetic casting, considering general geometries as objective.

Acknowledgements

The authors thank the Brazilian Research Councils CAPES, CNPq and Faperj, the Uruguayan National Research and Innovation Agency (ANII) and the French Research Councils COFECUB, INRIA and CNRS for the financial support.

References

- [1] C. Zhiqiang, J. Fei, Z. Xingguo, H. Hai, J. Junze, Microstructures and mechanical characteristics of electromagnetic casting and direct-chill casting 2024 aluminum alloys, *Materials Science and Engineering A* 327 (2) (2002) 133–137. doi:10.1016/S0921-5093(01)01673-2.
- [2] H. Z. Fu, J. Shen, L. Liu, Q. T. Hao, S. M. Li, J. S. Li, Electromagnetic shaping and solidification control of Ni-base superalloys under vacuum, *Journal of Materials Processing Technology* 148 (1) (2004) 25–29. doi:10.1016/j.jmatprotec.2003.11.039.
- [3] H. K. Moffatt, Magnetostatic equilibria and analogous Euler flows of arbitrarily complex topology. Part 1. Fundamentals, *Journal of Fluid Mechanics* 159 (1985) 359–378. doi:10.1017/S0022112085003251.
- [4] J. A. Shercliff, Magnetic shaping of molten metal columns, *Royal Society of London Proceedings Series A* 375 (1981) 455–473.

- [5] A. Henrot, J.-P. Brancher, M. Pierre, Existence of equilibria in electromagnetic casting, in: Proceedings of the Fifth International Symposium on Numerical Methods in Engineering, Vol. 1, 2 (Lausanne, 1989), Comput. Mech., Southampton, 1989, pp. 221–228.
- [6] A. Canelas, J. R. Roche, J. Herskovits, The inverse electromagnetic shaping problem, *Structural and Multidisciplinary Optimization* 38 (4) (2009) 389–403. doi:10.1007/s00158-008-0285-9.
- [7] A. Canelas, J. R. Roche, J. Herskovits, Inductor shape optimization for electromagnetic casting, *Structural and Multidisciplinary Optimization* 39 (6) (2009) 589–606. doi:10.1007/s00158-009-0386-0.
- [8] J. R. Roche, J. Sokołowski, Numerical methods for shape identification problems, *Control and Cybernetics* 25 (5) (1996) 867–894, shape optimization and scientific computations (Warsaw, 1995).
- [9] A. Friedman, M. Vogelius, Identification of small inhomogeneities of extreme conductivity by boundary measurements: a theorem on continuous dependence, *Archive for Rational Mechanics and Analysis* 105 (4) (1989) 299–326.
- [10] M. Brühl, M. Hanke, M. Vogelius, A direct impedance tomography algorithm for locating small inhomogeneities, *Numerische Mathematik* 93 (4) (2003) 635–654.
- [11] J.-P. Brancher, O. E. Séro-Guillaume, Étude de la déformation d’un liquide magnétique, *Archive for Rational Mechanics and Analysis* 90 (1) (1985) 57–85. doi:10.1007/BF00281587.
- [12] A. Gagnoud, J. Etay, M. Garnier, Le problème de frontière libre en lévitation électromagnétique, *Journal de Mécanique Théorique et Appliquée* 5 (6) (1986) 911–934.
- [13] A. Henrot, M. Pierre, Un problème inverse en formage des métaux liquides, *RAIRO Modélisation Mathématique et Analyse Numérique* 23 (1) (1989) 155–177.
- [14] A. Novruzi, J. R. Roche, Second order derivatives, Newton method, application to shape optimization, Tech. Rep. RR-2555, INRIA (1995).

- [15] M. Pierre, J. R. Roche, Computation of free surfaces in the electromagnetic shaping of liquid metals by optimization algorithms, *European Journal of Mechanics. B Fluids* 10 (5) (1991) 489–500.
- [16] M. Pierre, J. R. Roche, Numerical simulation of tridimensional electromagnetic shaping of liquid metals, *Numerische Mathematik* 65 (1) (1993) 203–217. doi:10.1007/BF01385748.
- [17] J.-C. Nédélec, *Acoustic and Electromagnetic Equations. Integral Representations for Harmonic Problems*, Vol. 144 of *Applied Mathematical Sciences*, Springer-Verlag, New York, 2001.
- [18] K. E. Atkinson, *The numerical solution of integral equations of the second kind*, Vol. 4 of *Cambridge Monographs on Applied and Computational Mathematics*, Cambridge University Press, Cambridge, 1997. doi:10.1017/CBO9780511626340.
- [19] J. Sokołowski, A. Żochowski, On the topological derivative in shape optimization, *SIAM Journal on Control and Optimization* 37 (4) (1999) 1251–1272.
- [20] G. Allaire, F. de Gournay, F. Jouve, A. Toader, Structural optimization using topological and shape sensitivity via a level set method, *Control and Cybernetics* 34 (1) (2005) 59–80.
- [21] S. Amstutz, H. Andrä, A new algorithm for topology optimization using a level-set method, *Journal of Computational Physics* 216 (2) (2006) 573–588.
- [22] S. Amstutz, S. Giusti, A. Novotny, E. de Souza Neto, Topological derivative in multi-scale linear elasticity models applied to the synthesis of microstructures, *International Journal for Numerical Methods in Engineering* To appear.
- [23] S. Amstutz, A. Novotny, Topological optimization of structures subject to von mises stress constraints, *Structural and Multidisciplinary Optimization* 41 (3) (2010) 407–420.
- [24] M. Burger, B. Hackl, W. Ring, Incorporating topological derivatives into level set methods, *Journal of Computational Physics* 194 (1) (2004) 344–362.

- [25] A. Novotny, R. Feijóo, E. Taroco, C. Padra, Topological sensitivity analysis for three-dimensional linear elasticity problem, *Computer Methods in Applied Mechanics and Engineering* 196 (41-44) (2007) 4354–4364.
- [26] S. Amstutz, I. Horchani, M. Masmoudi, Crack detection by the topological gradient method, *Control and Cybernetics* 34 (1) (2005) 81–101.
- [27] G. Feijóo, A new method in inverse scattering based on the topological derivative, *Inverse Problems* 20 (6) (2004) 1819–1840.
- [28] B. Guzina, M. Bonnet, Small-inclusion asymptotic of misfit functionals for inverse problems in acoustics, *Inverse Problems* 22 (5) (2006) 1761–1785.
- [29] M. Hintermüller, A. Laurain, Electrical impedance tomography: from topology to shape, *Control and Cybernetics* 37 (4) (2008) 913–933.
- [30] M. Masmoudi, J. Pommier, B. Samet, The topological asymptotic expansion for the Maxwell equations and some applications, *Inverse Problems* 21 (2) (2005) 547–564.
- [31] D. Auroux, M. Masmoudi, L. Belaid, Image restoration and classification by topological asymptotic expansion, in: *Variational formulations in mechanics: theory and applications*, Barcelona, Spain, 2007.
- [32] L. Belaid, M. Jaoua, M. Masmoudi, L. Siala, Application of the topological gradient to image restoration and edge detection, *Engineering Analysis with Boundary Element* 32 (11) (2008) 891–899.
- [33] M. Hintermüller, Fast level set based algorithms using shape and topological sensitivity, *Control and Cybernetics* 34 (1) (2005) 305–324.
- [34] M. Hintermüller, A. Laurain, Multiphase image segmentation and modulation recovery based on shape and topological sensitivity, *Journal on Mathematical Imaging and Vision* 35 (2009) 1–22.
- [35] I. Larrabide, R. Feijóo, A. Novotny, E. Taroco, Topological derivative: a tool for image processing, *Computers & Structures* 86 (13-14) (2008) 1386–1403.
- [36] S. Amstutz, Sensitivity analysis with respect to a local perturbation of the material property, *Asymptotic Analysis* 49 (1-2) (2006) 87–108.

- [37] S. Amstutz, A. Novotny, Topological asymptotic analysis of the Kirchhoff plate bending problem, ESAIM: Control, Optimisation and Calculus of Variations To appear.
- [38] J. R. de Faria, A. Novotny, On the second order topological asymptotic expansion, Structural and Multidisciplinary Optimization 39 (2009) 547–555.
- [39] G. Frémiot, W. Horn, A. Laurain, M. Rao, J. Sokołowski, On the analysis of boundary value problems in nonsmooth domains, Dissertationes Mathematicae (Rozprawy Matematyczne) 462 (2009) 149.
- [40] S. Garreau, P. Guillaume, M. Masmoudi, The topological asymptotic for pde systems: the elasticity case, SIAM Journal on Control and Optimization 39 (6) (2001) 1756–1778.
- [41] I. Hlaváček, A. Novotny, J. Sokołowski, A. Żochowski, On topological derivatives for elastic solids with uncertain input data, Journal Optimization Theory and Applications 141 (3) (2009) 569–595.
- [42] A. Khludnev, A. Novotny, J. Sokołowski, A. Żochowski, Shape and topology sensitivity analysis for cracks in elastic bodies on boundaries of rigid inclusions, Journal of the Mechanics and Physics of Solids 57 (10) (2009) 1718–1732.
- [43] T. Lewinski, J. Sokołowski, Energy change due to the appearance of cavities in elastic solids, International Journal of Solids and Structures 40 (7) (2003) 1765–1803.
- [44] S. Nazarov, J. Sokołowski, Asymptotic analysis of shape functionals, Journal de Mathématiques Pures et Appliquées 82 (2) (2003) 125–196.
- [45] S. Nazarov, J. Sokołowski, Self-adjoint extensions of differential operators in application to shape optimization, C. R. Mecanique 331 (2003) 667–672.
- [46] S. Nazarov, J. Sokołowski, Singular perturbations in shape optimization for the Dirichlet laplacian, C. R. Mecanique 333 (2005) 305–310.
- [47] S. Nazarov, J. Sokołowski, Self-adjoint extensions for the Neumann laplacian and applications, Acta Mathematicae Applicatae Sinica 22 (3) (2006) 879–906.

- [48] J. Sokołowski, Optimality conditions for simultaneous topology and shape optimization, *SIAM Journal on Control and Optimization* 42 (4) (2003) 1198–1221.
- [49] J. Sokołowski, A. Żochowski, Modelling of topological derivatives for contact problems, *Numerische Mathematik* 102 (1) (2005) 145–179.
- [50] C. R. Sullivan, Optimal choice for number of strands in a litz-wire transformer winding, *IEEE Transactions On Power Electronics* 14 (2) (1999) 283–291.
- [51] T. P. Felici, J.-P. Brancher, The inverse shaping problem, *European Journal of Mechanics. B Fluids* 10 (5) (1991) 501–512.
- [52] A. Novotny, R. Feijóo, C. Padra, E. Taroco, Topological sensitivity analysis, *Computer Methods in Applied Mechanics and Engineering* 192 (7-8) (2003) 803–829.
- [53] M. Delfour, J. Zolésio, *Shapes and Geometries. Advances in Design and Control*, SIAM, Philadelphia, 2001.
- [54] J. Sokołowski, J. Zolésio, *Introduction to shape optimization - shape sensitivity analysis*, Springer-Verlag, New York, 1992.
- [55] G. Hsiao, W. L. Wendland, *Boundary Integral Equations*, Vol. 164 of *Applied Mathematical Sciences*, Springer-Verlag, Berlin, 2008.
- [56] C. A. Brebbia, J. C. F. Telles, L. C. Wrobel, *Boundary Element Technique: Theory and Applications in Engineering*, Springer-Verlag, 1984.
- [57] C. A. Brebbia, J. Dominguez, *Boundary elements: an introductory course*, 2nd Edition, Computational Mechanics Publications, Southampton, 1992.